Multilayered tissue mimicking skin and vessel phantoms with tunable mechanical, optical, and acoustic properties

Alvin I. Chen[a] and Max L. Balter
Department of Biomedical Engineering, Rutgers University, Piscataway, New Jersey 08854

Melanie I. Chen
Ernest Mario School of Pharmacy, Rutgers University, Piscataway, New Jersey 08854

Daniel Gross
Riverside Research Institute, Piscataway, New York, New York 10038

Sheikh K. Alam
Center for Computational Biomedicine Imaging and Modeling, Rutgers University, Piscataway, New Jersey 08854

Timothy J. Maguire
VascuLogic, L.L.C., Piscataway, New Jersey 08854

Martin L. Yarmush
Department of Biomedical Engineering, Rutgers University, Piscataway, New Jersey 08854

(Received 22 September 2015; revised 1 May 2016; accepted for publication 10 May 2016; published 27 May 2016)

Purpose: This paper describes the design, fabrication, and characterization of multilayered tissue mimicking skin and vessel phantoms with tunable mechanical, optical, and acoustic properties. The phantoms comprise epidermis, dermis, and hypodermis skin layers, blood vessels, and blood mimicking fluid. Each tissue component may be individually tailored to a range of physiological and demographic conditions.
Methods: The skin layers were constructed from varying concentrations of gelatin and agar. Synthetic melanin, India ink, absorbing dyes, and Intralipid were added to provide optical absorption and scattering in the skin layers. Bovine serum albumin was used to increase acoustic attenuation, and 40 μm diameter silica microspheres were used to induce acoustic backscatter. Phantom vessels consisting of thin-walled polydimethylsiloxane tubing were embedded at depths of 2–6 mm beneath the skin, and blood mimicking fluid was passed through the vessels. The phantoms were characterized through uniaxial compression and tension experiments, rheological frequency sweep studies, diffuse reflectance spectroscopy, and ultrasonic pulse-echo measurements. Results were then compared to *in vivo* and *ex vivo* literature data.
Results: The elastic and dynamic shear behavior of the phantom skin layers and vessel wall closely approximated the behavior of porcine skin tissues and human vessels. Similarly, the optical properties of the phantom tissue components in the wavelength range of 400–1100 nm, as well as the acoustic properties in the frequency range of 2–9 MHz, were comparable to human tissue data. Normalized root mean square percent errors between the phantom results and the literature reference values ranged from 1.06% to 9.82%, which for many measurements were less than the sample variability. Finally, the mechanical and imaging characteristics of the phantoms were found to remain stable after 30 days of storage at 21 °C.
Conclusions: The phantoms described in this work simulate the mechanical, optical, and acoustic properties of human skin tissues, vessel tissue, and blood. In this way, the phantoms are uniquely suited to serve as test models for multimodal imaging techniques and image-guided interventions.
 [http://dx.doi.org/10.1118/1.4951729]

Key words: tissue mimicking phantom, mechanical properties, optical properties, acoustic properties, multimodality imaging

1. INTRODUCTION

Skin and vessel phantoms have been widely used as test models for a variety of peripheral tissue imaging techniques and image-guided interventions. These phantoms consist of a skin mimicking material surrounding a vessel through which blood mimicking fluid (BMF) is perfused. An important criterion for the phantoms is that the individual components should have similar material properties to soft tissue, vessel tissue, and blood. Of particular interest are phantoms designed to eval-

uate multimodality techniques such as photoacoustic imaging, elastography-based imaging, and percutaneous needle insertion.[1–3] For such applications, the mechanical, optical, and acoustic properties of the peripheral tissues must all be reproduced, and this greatly increases the complexity of the phantoms.

The literature on tissue mimicking phantom materials is extensive,[4–6] and over the years a number of customizable multimodal phantoms have been described. Recently, Lamouche *et al.* provided a comprehensive review of phantoms with controllable optical, mechanical, and structural properties for optical coherence elastography.[7] Their focus was on the effects of different substrates (silicone, fibrin, and polyvinyl alcohol) on optical scattering behavior and mechanical strength. Madsen *et al.* demonstrated the use of gelatin/agar phantoms for ultrasonic elastography. They investigated the effects of India ink, Intralipid, glycerol, and graphite powder on the acoustic and mechanical properties of the phantoms.[8,9] Cook *et al.* reported on the design of gelatin-based phantoms for photoacoustic imaging.[10] The phantoms used India ink and dyes as the optical absorbers, Intralipid as the optical scatterer and acoustic attenuator, and silica microspheres as the acoustic backscattering agent. In their study, the phantoms were developed as single-component, homogenous bulk materials, and the mechanical properties were not investigated. Hungr *et al.* developed a deformable polyvinyl chloride prostate phantom for multimodal imaging and percutaneous needle insertion procedures, and characterized the sound velocity, mechanical properties, and effects of long-term storage.[11] In addition to general tissue mimicking materials, phantoms with vessel-like geometries have also been introduced. Such phantoms have been developed using materials such as thin-walled silicone tubing,[12] polyvinyl alcohol gels,[13,14] and gelatin/agar hydrogels.[15,16]

In this paper, we focus on the design, fabrication, and characterization of multilayered phantoms that mimic the mechanical, optical, and acoustic properties of five peripheral tissues, namely the epidermis, dermis, hypodermis, blood vessels, and blood [Fig. 1(a)]. Uniaxial compression and tension experiments are performed to measure the Young's modulus E of each phantom tissue component at strains up to 1.0 and strain rates of 10^{-3}–10^{1} s^{-1}. Rheological frequency sweep experiments are conducted to determine dynamic shear modulus G at shear strain rates of 10^{-2}–10^{2} s^{-1}. Optical absorption μ_a and scattering μ_s' are measured in the wavelength range of 400–1100 nm by diffuse reflectance spectroscopy. Finally, acoustic attenuation α, backscatter β, speed of sound c, mass density ρ, and acoustic impedance Z are determined in the fre-

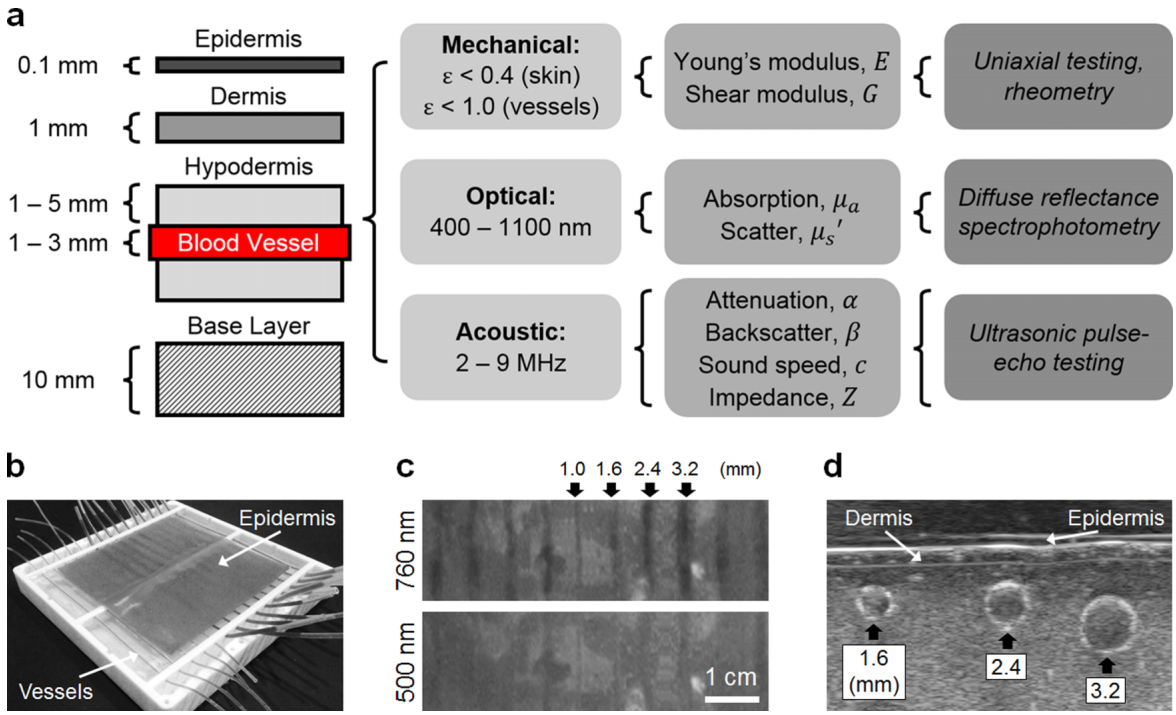

FIG. 1. Design and characterization of skin and vessel mimicking phantoms. (a) *Far left*: The phantoms comprise a 0.1 mm thick epidermis mimicking layer, a 1 mm thick dermis layer, and a 10 mm thick hypodermis layer. Blood vessel substitutes with diameters between 1 and 3.2 mm are embedded at varying depths within the hypodermis. Blood mimicking fluid is perfused through the vessels. *Left center*: The phantoms simulate the mechanical properties of human skin and vessel tissues for strains up to 0.4 and 1.0, respectively; optical properties between 400 and 1100 nm; and acoustic properties between 2 and 9 MHz. *Right center*: Eight material properties were assessed, and the results were compared to human tissue values from the literature. *Far right*: Experimental techniques used to characterize the material properties of each phantom tissue component. (b) Completed phantom containing 15 vessels. To aid in visualization of the embedded vessels, absorbers and scatterers were not added to the dermis or hypodermis layers in the photographed phantom and the epidermis layer was cut to a smaller size. (c) Images taken at 500 and 760 nm showing vessels with varying diameters embedded at a depth of 3 mm below the skin surface. The difference in image contrast between the two wavelengths can be observed. (d) Transverse ultrasound image of phantom acquired at 9 MHz showing the individual skin layers and vessels.

quency range of 2–9 MHz using single-element transducers. The results are compared to *in vivo* and *ex vivo* tissue data from the literature.

2. PHANTOM DESIGN AND FABRICATION

2.A. Fabrication procedure

Tables I and II summarize the design and material composition, respectively, of each phantom tissue mimicking component. Phantoms were fabricated in 3D-printed square containers ($120\times120\times21$ mm) [Fig. 1(b)]. Flexible and transparent thin-walled polydimethylsiloxane (PDMS) tubing (Sylgard 184 Silicone Elastomer Laboratory Tubing, Dow-Corning Corp., MI, USA) were cut to 150 mm in the length and used as blood vessel substitutes. The vessels had diameters ranging from 1 to 3.2 mm and a wall thickness of 0.4 mm [Figs. 1(b)–1(d)], and were anchored by slots cut into two opposing walls of the phantom container. The depth of each vessel was fixed between 2 and 6 mm from the top of the container and was determined by the position of each slot. The skin mimicking layers were then fabricated and introduced into the phantom as described below.

TABLE I. Summary of the material properties ($E, G, \mu_a, \mu_s', \alpha, \beta, c, Z$, and η) investigated in this study. Also shown are the constituent materials that make up the peripheral tissue layers in both humans and phantoms.

Tissue layer	Material property	Human tissue components	Phantom tissue modifiers
Epidermis	E, G	Keratin	Gelatin (films)
	μ_a	Melanin	Synthetic melanin
	μ_s'	Melanin	Synthetic melanin
	α	Keratin, melanin	IL-20, BSA
	β	Keratin, melanin	40 μm silica beads
	c, Z	Keratin, melanin	Glycerol
Dermis	E, G	Collagen/elastin	Gelatin, agar
	μ_a	Hemoglobin	India ink, 552 nm dye
	μ_s'	Collagen/elastin	IL-20
	α	Collagen/elastin	IL-20, BSA
	β	Collagen/elastin	40 μm silica beads
	c and Z	Collagen/elastin	Methanol
Hypodermis	E, G	Adipose	Gelatin, agar
	μ_a	Adipose, hemoglobin	India ink, 935 nm dye
	μ_s'	Adipose	IL-20
	α	Adipose	IL-20, BSA
	β	Adipose	40 μm silica beads
	c and Z	Adipose	Methanol
Vessel wall	E, G	Collagen/elastin	PDMS
	μ_a	Hemoglobin	Negligible
	μ_s'	Collagen/elastin	Negligible
	α	Collagen/elastin	PDMS
	β	Collagen/elastin	Negligible
	c and Z	Collagen/elastin	PDMS
Whole blood	η	RBCs	Glycerol, dextran
	μ_a	Hemoglobin	552/757/912 nm dyes
	μ_s'	RBCs	Negligible
	α	Hemoglobin, plasma	Negligible
	β	RBCs	5 μm polyamide beads
	c and Z	RBCs, plasma	Glycerol, dextran

2.A.1. Fabrication of phantom epidermis layers

Epidermis mimicking films with thickness of 0.1 mm were prepared by dissolving 10 g gelatin powder (Type A porcine powder, 300 g Bloom, Sigma-Aldrich, Corp., MO, USA) and 5 g glycerol (49781, ≥98% purity, Sigma-Aldrich) in 100 ml of distilled water. 0.01%–0.1% glutaraldehyde (G5882, ≥99.5% purity, Sigma-Aldrich) was then added to the solutions, along with varying concentrations of synthetic melanin (described later). The solutions were poured onto a 12×12 cm Plexiglas plate and dried for 48 h at 21 °C and 28% relative humidity to obtain the thin films.

2.A.2. Fabrication of phantom dermis and hypodermis layers

The dermis mimicking layer was fabricated from a mixture of 24% gelatin and 1% agar (A1296 powder, Sigma-Aldrich), while the hypodermis mimicking layer consisted of 2% gelatin and 0.2% agar. A base layer of 8% gelatin was also formed. The gelatin and agar powders were dissolved in separate beakers and then combined, and optical and acoustic modifiers were added (described later) along with 1.5% Germall-Plus (International Specialty products, Wayne, NJ, USA), which served as an antimicrobial agent.[9] The final solutions were cooled to 40 °C under constant stirring and introduced into the phantom container sequentially. The base layer was first introduced by pouring 8% gelatin solution through a 100 μm sieve (BD Falcon™ Cell Strainer) until a 10 mm thick viscous layer was formed a the bottom of the container. Depending on the height of the vessels, between 1 and 5 mm of spacing remained between the base layer and the vessels. Once the base layer was fully gelled, the hypodermis solution was then added to a total height of 20 mm, allowing the vessels to be fully submerged. After the hypodermis layer was gelled, the dermis solution was added to form a 1 mm layer. Finally, once the dermis layer was gelled, the epidermis film was placed above the dermis to form the topmost layer of the phantom.

2.A.3. Introduction of blood mimicking fluid

A commercial BMF (Model 046 Blood Mimicking Fluid, CIRS, Inc., VA, USA) described by Ramnarine *et al.*[17,18] was used here. The BMF consists of a (water/glycerol)/dextran base and 10 μm polyamide microspheres that mimic the acoustic backscatter of RBCs. The BMF may be passed through the vessels at controlled velocities during experiments, using, for example, a syringe pump to simulate continuous blood flow in the veins or a peristaltic pump to simulate pulsatile flow in the arteries.

2.B. Modification of phantom optical properties

The main component materials that affect the optical properties of peripheral tissues include melanin in the epidermis,

TABLE II. Percent concentrations of phantom components used for each tissue mimicking layer.

Tissue layer	Gelatin (% v)	Agar (% w/v)	Melanin (% w/v)	Absorbing dyes (% w/v)	India ink (% v/v)	IL-20 (% v/v)	BSA (% w/v)	Silica beads (% w/v)	Other
Material properties affected	E, G μ_a (minor) α (minor)	E, G	μ_a μ_s'	μ_a	μ_a	$\mu_s'\alpha$	α μ_s' (minor)	β μ_s' (minor)	
Epidermis	5	—	0.0003 (1% φ_{mel}) 0.0015 (5% φ_{mel}) 0.0030 (10% φ_{mel}) 0.0047 (15% φ_{mel}) 0.0102 (30% φ_{mel}) 0.0216 (45% φ_{mel})	—	—	—	—	—	0.01%–0.1% glutaraldehyde
Dermis	24	1	—	0.058 (552 nm)	0.0182	28.5	35	1.0	15.31% methanol
Hypodermis	2	0.2	—	0.073 (552 nm) 0.047 (935 nm)	0.0202	7.8	15	0.5	23.45% methanol
Vessels	—	—	—	—	—	—	—	—	Commercial PDMS tubing
Blood (venous)	—	—	—	23.19 (552 nm) 1.373 (756 nm) 0.214 (935 nm)	0.0301	—	—	—	Commercial blood mimicking fluid
Blood (arterial)	—	—	—	26.09 (552 nm) 0.374 (935 nm)	0.0301	—	—	—	Commercial blood mimicking fluid
Notes	Gelatin concentration for epidermis layer based on weight % before drying	Calculated as weight % of Sigma-Aldrich A1296 agar powder	Calculated as weight % of Sigma-Aldrich M0418 synthetic melanin powder, ≥97% purity	Absorptivity at 552, 756, and 935 nm: 138, 52, and 187 l g^{-1} cm^{-1}, respectively	Calculated as volume % of undiluted Higgins waterproof black ink	Calculated as volume % of undiluted Fresenius- Kabi IL-20%	Calculated as weight % of Roche lyophilized BSA, ≥95% purity	Calculated as weight % of 40 μm diameter MIN-U-SIL silica microspheres	

TABLE III. Relative composition of human tissues used to inform phantom designs.

	Volume percentages (φ) of tissue components				
Tissue layer	Melanin (%)	Collagen, elastin (%)	Lipid (%)	Hemoglobin (%)	Water (%)
Epidermis	0–45	40	0	<1	15–60
Dermis	0	50	0	<1	50
Hypodermis	0	0	80	<1	20
Vessel wall	0	25	0	<1	75
Whole blood	0	0	0	2	98

collagen, and elastin in the dermis, lipid in the hypodermis, hemoglobin in blood, and water[19,20] (Table III). Optical absorption over the wavelength range of 400–1100 nm may be estimated as the sum of the individual absorption profiles μ_a^m of each component material m in the tissue and their relative percent volumes φ_m, that is, $\mu_a = \sum_m^n \varphi_m \mu_a^m$ [Eq. (1)]. Unlike with absorption, total optical scattering in the tissue is not necessarily equal to the sum of the individual scattering components. Rather, scattering in tissues may be approximated by a power law expression, $\mu_s' = \mu_{s_1}'(\lambda/500)^{-n_s}$, where μ_{s_1}' is the reduced scattering coefficient at 1 nm and n_s is the power law constant describing the dependence on wavelength.[19]

2.B.1. Controlling optical absorption and scattering in the phantom epidermis

Absorption and scattering in the epidermis are primarily due to melanin.[21] In the phantom epidermis layer, synthetic melanin powder (M0418, ≥97% purity, Sigma-Aldrich Corporation, USA) was added at concentrations ranging from 0.0003% to 0.0216% to simulate different skin tones. The optical properties of the brand of melanin used in this study has been described in detail by Bashkatov *et al.*[22] An advantage of using synthetic melanin is that its index of refraction (~1.65) is relatively similar to that of epidermis tissue (~1.44) compared to other absorbers.[23] Furthermore, because melanin is a strong optical scatterer, additional scattering materials are not needed.

2.B.2. Controlling optical absorption in the phantom dermis and hypodermis

Dermis tissue consists of weak absorbers (collagen, elastin, and minor amounts of hemoglobin), and so absorption is relatively low (<1 cm^{-1}).[24] In hypodermis tissue, absorption is highest at the fat absorption peaks (e.g., at 935 nm) and low elsewhere.[25] We used India ink (Higgins Waterproof Black, Sanford, USA) as the broad-spectrum absorber in the phantom dermis and hypodermis layers, and molecular absorbing dyes (QCR Solutions Corp., FL, USA) to simulate local absorption peaks. Specifically, 0.0182% of India ink and 0.058% of 552 nm dye were added to the dermis, while 0.0182% of India ink 0.047% of 935 nm dye was added to the hypodermis. The 552 and 935 nm dyes were added to simulate the increase in absorption due to hemoglobin and lipid, respectively. The India ink concentrations were determined based on absorption measurements reported by others using the same brand of ink,[26] while the dye concentrations were determined from material data sheets.

2.B.3. Controlling optical scattering in the phantom dermis and hypodermis

The presence of collagen and elastin fibers leads to strong optical scattering in the dermis,[24] while in the hypodermis the main scatterers are the lipid droplets.[25] To simulate the scattering profile of human skin, 28.5% and 7.8% Intralipid-20% (IL-20, Fresenius Kaby AB, Sweden) were added as the optical scatterer in the dermis and hypodermis, respectively. Cook *et al.* have characterized the scattering properties of IL-20, noting that μ_s' is diminished in gelatin compared to water and thus higher concentrations are needed;[10] this decrease in scattering was accounted for when determining IL-20 concentrations for the phantom tissue components. Meanwhile other studies have shown that absorption of IL-20 is negligible, that minimal variability (<2%) is exhibited between brands, batches, and over time, and that IL-20 does not affect the absorption properties of India ink, nor vice versa.[27,28]

2.B.4. Controlling optical absorption in blood mimicking fluid

To reproduce the optical absorption of venous and arterial blood, molecular absorbing dyes (QCR Solutions Corp., FL, USA) and India ink were added to the commercial BMF. Specifically, dyes with absorption maxima at 552, 757, and 912 nm were used, while India ink provided the baseline absorption. (Colored inks such as Congo Red and Evans Blue may be used as low-cost alternatives to the molecular dyes.[10])

2.C. Modification of phantom acoustic properties

Acoustic attenuation in most human tissues is known to increase with frequency following the power law function $\alpha = \alpha_1 f^{n_\alpha}$ dB cm^{-1}, where α_1 is the attenuation coefficient at 1 MHz, n_α is the power constant, and f is the frequency.[29] Similarly, acoustic backscatter may be modeled as $\beta = \beta_1 f^{n_\beta}$ (sr^{-1} cm^{-1}), where β_1 is the backscatter coefficient and n_β is the power constant. On the other hand, we assumed that speed of sound and acoustic impedance were constants with respect to frequency (valid for human tissues).

2.C.1. Controlling acoustic attenuation and backscatter in phantom tissues

Gelatin, agar, and IL-20 are all weak acoustic attenuators,[9,10,30] and thus the addition of a modifier with strong attenuating properties is needed. Unfortunately, most attenuators affect the optical and/or mechanical properties of the materials to some extent. An exception is bovine serum albumin (BSA),

which is optically transparent when dissolved in aqueous solution. The attenuation coefficient α_1 of 1% BSA is ~0.02 dB cm^{-1} MHz^{-1} and increases linearly with concentration.[31,32] Here we added 35% lyophilized BSA (≥95% purity, Roche Diagnostics, USA), which was expected to raise α_1 in the dermis layer from ~0.5 to ~1.1 dB cm^{-1} MHz^{-1}. Similarly, 15% BSA was added to the hypodermis layer to raise α_1 from ~0.3 to ~0.6 dB cm^{-1} MHz^{-1}. In both layers, BSA was slowly dissolved into solution at 30 °C, which is well below its denaturing temperature. BSA was not added to the epidermis layer, vessels, or blood.

To modify the acoustic backscatter parameters in the dermis and hypodermis, 40 μm diameter monodisperse silica microspheres (MIN-U-SIL-4, Sigma-Alrich) were added at 0.5% and 1%, respectively. At such concentrations, the backscatter coefficient β_1 was expected to be on the order of 10^{-3} sr^{-1} cm^{-1} MHz^{-1}, which is in the range of human skin and fatty tissues.[10] As with BSA, the silica spheres were chosen over alternative materials due to their optical transparency.

2.C.2. Controlling speed of sound (and acoustic impedance) in phantom tissues

Varying the gelatin concentration from 2% to 24% has been shown to increase speed of sound linearly from 1490 to 1560 m s^{-1} (increase of ~3.2 m s^{-1} for each percent of gelatin added).[10] Similarly, increasing the agar concentration from 0.2% to 2% increases speed of sound linearly from 1482 to 1500 m s^{-1} (~1 m s^{-1}/0.1% agar).[30] Likewise, BSA has been observed to increase speed of sound by ~3 m s^{-1} for each percent added.[31,32] In contrast to the above materials, IL-20 has minimal effect on sound speed,[10] and the other modifiers (India ink, absorbing dyes, and silica beads) were all present in very low concentrations (≤1%) and thus were not expected to significantly affect speed of sound.

Based on the material composition of the phantom skin layers, the estimated speed of sound and acoustic impedance in the dermis layer ($c \sim 1642$ m s^{-1}, $Z \sim 1.7 \times 10^6$ kg m^{-2} s^{-1}) and hypodermis layer ($c \sim 1522$ m s^{-1}, $Z \sim 1.7 \times 10^6$ kg m^{-2} s^{-1}) were expected to be higher than measurements on human dermis ($c \sim 1595$ m s^{-1}, $Z \sim 1.7 \times 10^6$ kg m^{-2} s^{-1}) and hypodermis ($c \sim 1450$ m s^{-1}, $Z \sim 1.7 \times 10^6$ kg m^{-2} s^{-1}).[33,34] To compensate for this, methanol was introduced into the dermis and hypodermis layers at concentrations of 15.31% and 23.45%, respectively. Methanol is known to decrease speed of sound by 3.77 m s^{-1} for each percent added, and like BSA causes no measureable changes to the optical or mechanical properties of the material.[6,8]

Meanwhile, the estimated speed of sound and impedance in the epidermis layer ($c \sim 1625$ m s^{-1}, $Z \sim 1.7 \times 10^6$ kg m^{-2} s^{-1}) was expected to remain in range of measurements on human epidermis ($c \sim 1645$ m s^{-1}, $Z \sim 1.7 \times 10^6$ kg m^{-2} s^{-1}).[34] Finally, in the phantom vessels, acoustic properties were determined entirely by Sylgard 184 PDMS ($c \sim 1030$ m s^{-1}, $Z \sim 1.7 \times 10^6$ kg m^{-2} s^{-1}). These values are lower than measurements on human vessel wall tissue ($c \sim 1575$ m s^{-1}, $Z \sim 1.7 \times 106$ kg m^{-2} s^{-1}), and this disparity is a potential limitation of the commercial vessel substitutes.

In this study, the mass densities of the phantom tissue components were not independently modified. To the best of our knowledge, changes in mass density with respect to gelatin, IL-20, and BSA concentration have not yet been fully characterized in the literature.

2.D. Packaging and storage

The crosslinked epidermis layer helps to reduce drying of the dermis and hypodermis layers below. The addition of Germall-Plus further prolongs the shelf-life by mitigating microbial or fungal infiltration. The phantoms, once fully gelled in the 3D-printed containers, are wrapped in Saran Wrap and packaged in vacuum-sealed bags (FoodSaver V2244 Sealing System). The phantoms are then stored at room temperature (21 °C).

3. RESULTS

3.A. Phantom mechanical characterization

3.A.1. Elasticity of gelatin and agar gels at varying concentrations

We first measured the true stress vs strain responses of 2%, 4%, 8%, 12%, 16%, 20%, and 24% gelatin [Fig. 2(a)] and 0.1%, 0.5%, 1%, and 2% agar [Fig. 2(b)]. Measurements were obtained from unconfined uniaxial compression tests (ElectroForce 3200 Test Instrument, Bose Corp., MA, USA), and the gels were assumed to be incompressible. The gels were compressed to a strain of 0.5 at five strain rates (10^{-3}–10^{-1} s^{-1}), and Young's modulus was defined as the slope of the stress response in the low strain regime ($\varepsilon < 0.2$). For both types of gels, Young's modulus was seen to depend on both gel concentration and strain rate.

3.A.2. Thickness and elasticity of phantom dermis and hypodermis

Mean thickness values for the dermis and hypodermis phantom layers were 1.4 and 2.1 mm, respectively (Table IV). Measurements were made on four dermis samples and four hypodermis samples from B-mode images acquired with an 18 MHz ultrasound transducer (L1830, Telemed UAB, Lithuania). Stress vs strain responses were then obtained for the dermis and hypodermis samples [Figs. 2(c) and 2(d)]. At low strains ($\varepsilon < 0.2$), the stiffness of the phantoms was provided by the gelatin component, and the stretch behavior was linearly elastic. Young's modulus of the phantom dermis was ~50 kPa for strains below 0.2 (Table V) and approximated that of porcine dermis.[35] Similarly, the hypodermis phantom tissue was linearly elastic for strains below 0.2, and Young's modulus (~2 kPa) approximated that of porcine hypodermis tissue.[36] In contrast, for $\varepsilon > 0.2$, rapid strain hardening was observed in both the phantom and porcine skin tissues. In the phantoms, this nonlinear behavior was predominantly due to the agar component.

Following the addition of 28.5% IL-20% and 35% BSA, the Young's modulus of the dermis layer decreased by a mean of

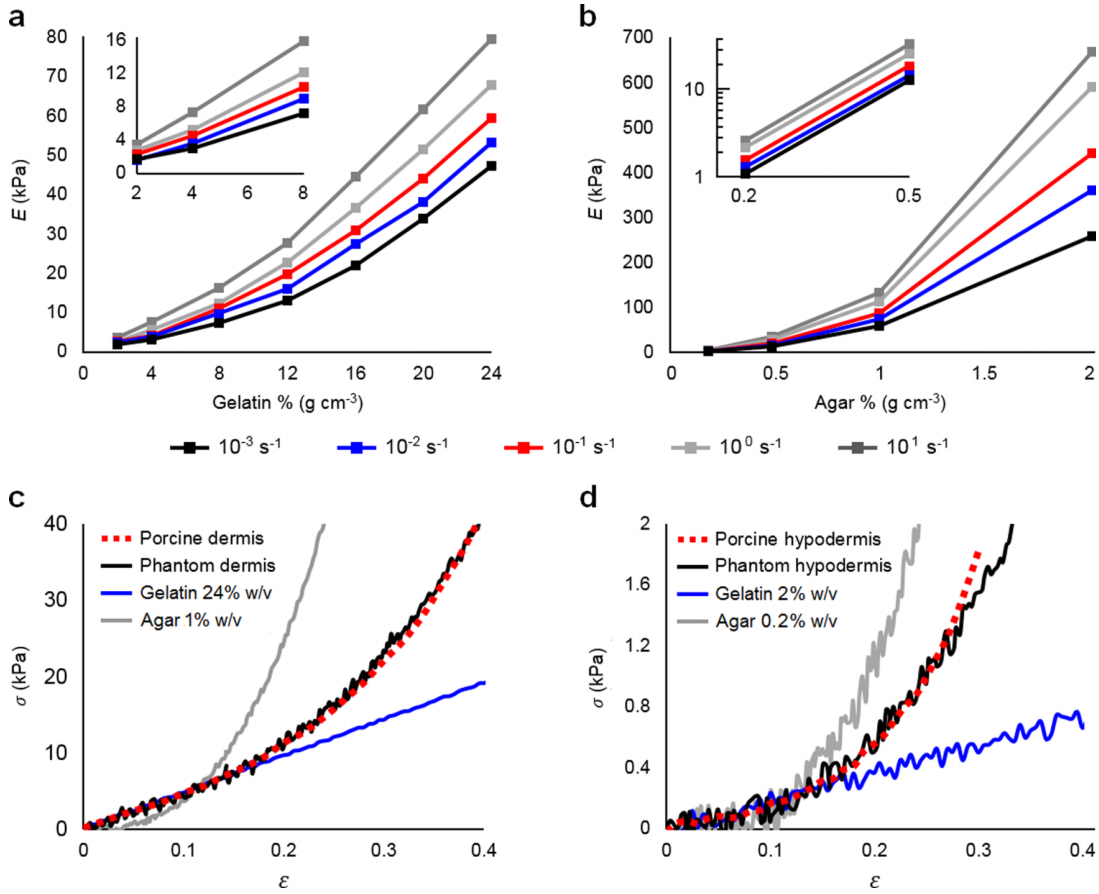

FIG. 2. Mechanical characterization of gelatin, agar, and skin phantoms. (a) Young's moduli E for 2%–24% gelatin, measured during uniaxial compression over five strain rates ($\dot{\varepsilon} = 10^{-3}$-$10^{1}$ s^{-1}). (b) Young's moduli E for 0.2%–2% agar ($\dot{\varepsilon} = 10^{-3}$-$10^{1}$ s^{-1}) from uniaxial compression. (c) Compressive true stress vs strain curves for dermis mimicking phantom layer in comparison to *ex vivo* porcine dermis (Ref. 35). Phantom and human measurements were both obtained from unconfined uniaxial compression tests at $\dot{\varepsilon} = 10^{1}$ s^{-1}. Pure gelatin exhibited perfectly linear elasticity for $\varepsilon < 0.5$ (blue line), while pure agar exhibited a highly nonlinear stress vs strain relationship (gray line). Phantoms combining 24% gelatin and 1% agar (black line) were found to most closely mimic porcine dermis tissue (red dotted line). (d) Compressive true stress vs strain curves for phantom hypodermis compared to *ex vivo* porcine hypodermis tissue (Ref. 36). Measurements were at $\dot{\varepsilon} = 10^{1}$ s^{-1}. Phantoms combining 2% gelatin and 0.2% agar most closely mimicked porcine hypodermis tissue. (See color online version.)

0.81 kPa over four samples. Similarly, the Young's modulus of the hypodermis phantom decreased by 0.22 kPa after adding 7.8% IL-20% and 15% kPa. However, in both cases, the differences were smaller than the variability between samples and thus were likely to be insignificant. The other modifiers were present in very low concentrations (≤1%) and were not expected to measurably alter the mechanical properties of the phantoms.

TABLE IV. Thickness, δ (in mm) of human and phantom skin, vessel wall, and blood.

Tissue layer	Phantom (mm)	Human (mm)	Body location (measurement technique)	Reference
Epidermis	0.117 ± 0.022	0.075 ± 0.016	Forearm	39
		0.095 ± 0.005	Forearm	40
		0.138 ± 0.013	Forearm	41
Dermis	1.385 ± 0.167	0.92 ± 0.12	Forearm	43
		1.14 ± 0.20	Forearm	44
		1.16 ± 0.16	Forearm	45
		1.35 ± 0.10	Forearm	46
Hypodermis	2.093 ± 0.514	1.21 ± 0.32	Forearm	45
		2.15 ± 0.64	Forearm	47
Vessel wall	1.19–3.18 (diameter)	2.1 ± 1.1 ($d$vein)	Forearm	48
		3.0 ± 0.8 ($d$artery)		
	0.28–0.51 (wall thickness)	0.31 ± 0.07 (δvein)		
		0.40 ± 0.08 (δartery)		

TABLE V. Young's modulus, E (in kPa) of human and phantom skin, vessel wall, and blood.

Tissue layer	Phantom (kPa)	Human (kPa)	Body location (measurement technique)	Reference
Epidermis	$0.997 \pm 0.138 \times 10^3$ ($\varepsilon < 0.2, \dot{\varepsilon} = 10^{-1}$ s^{-1})	$1–2 \times 10^3$	Abdomen (indentation)	40
Dermis	50.71 ± 2.982 ($\varepsilon < 0.1$, $\dot{\varepsilon} = 10^{-1}$ s^{-1})	35	Forearm (indentation)	49
		56	Forearm (suction)	41
		~50 ($\varepsilon > 0.1$)	Buttock, porcine (compression)	35
Hypodermis	1.76 ± 0.375 ($\varepsilon > 0.1$, $\dot{\varepsilon} = 10^{-1}$ s^{-1})	2	Forearm (indentation)	49
		1.6 ($\varepsilon < 0.1$)	Abdomen (tensile)	47
		1–2.5 ($\varepsilon < 0.1$)	Abdomen, porcine (compression)	45
Vessel wall	912.58 ± 11.32 ($\varepsilon < 0.5$, $\dot{\varepsilon} = 10^{-1}$ s^{-1})	0.5×10^3 (vein, $\varepsilon > 0.4$) 1.0×10^3 (artery, $\varepsilon < 0.4$)	Porcine (tensile)	48

3.A.3. Dynamic shear properties of phantom dermis and hypodermis

Figure 3 shows the frequency dependence of shear modulus in the dermis and hypodermis mimicking phantoms. Measurements were obtained from rheometry experiments (Ares G2 Rheometer, TA Instruments, USA) at a shear strain of 0.5 and shear rates ranging from 10^{-2} to 10^2 s^{-1}. The shear modulus of the phantoms were comparable to measurements on human skin tissues[37,38] (Table VI).

3.A.4. Thickness and elasticity of phantom epidermis

The mean thickness of the epidermis films over four samples was measured by ultrasound to be 0.12 mm, which is comparable to the thickness of the human epidermis.[39–41] Each film contained 0.0102% melanin, which corresponds to a melanin volume fraction φ_{mel} of 30% (see Table III). Figure 4 shows the Young's modulus of epidermis films crosslinked with 0.01%, 0.025%, 0.05%, 0.075%, or 0.1% glutaraldehyde. All films exhibited linearly elastic behavior under tensile stress until fracture at a strain of 0.2. The addition of 0.025% glutaraldehyde produced films with Young's modulus of ~1 MPa, which is comparable to indentation results on *ex vivo* human epidermis.[40]

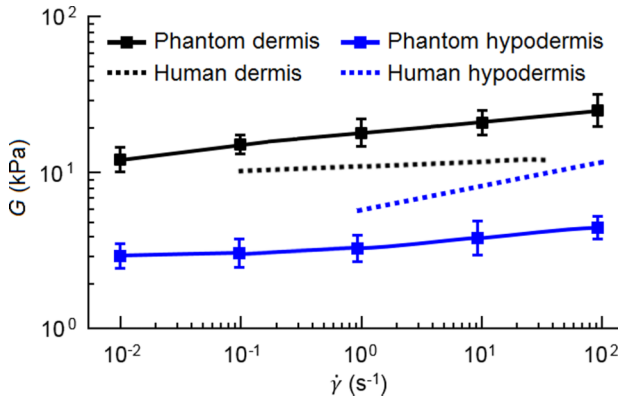

FIG. 3. Shear modulus G of phantom dermis (black) and hypodermis (blue). Measurements were obtained from rheological frequency sweep at a shear strain of 0.5. Shear strain rates were increased from 10^{-2} to 10^2 s^{-1}. The magnitude and strain rate dependence of the phantoms are comparable to those of human skin tissues (dotted lines) (Refs. 37 and 38). (See color online version.)

3.A.5. Diameter, wall thickness, and elasticity of phantom blood vessels

Figure 5 shows the results of uniaxial tension experiments performed over varying strain rates on the phantom vessels. Results were compared to tensile measurements on *ex vivo* human venous and arterial wall[42] (Fig. 5). At strains below 0.5, the vessels were linearly elastic and Young's modulus was ~1 MPa. At strains above 0.5, strain hardening was observed.

3.B. Phantom optical characterization

Measurements of transmittance and diffuse reflectance were obtained for the epidermis, dermis, and hypodermis mimicking phantom layers in the 400–1100 nm wavelength range using a commercial spectrophotometer (HR4000 UV-NIR, Ocean Optics, Inc., FL, USA) coupled to an integrating sphere (IS200-4 2," Thorlabs, Inc., NJ, USA). The inverse adding-doubling method[51] was applied to determine absorption and reduced scattering coefficients (μ_a and μ_s', respectively) (Table VII) from the transmittance and reflectance data.

3.B.1. Optical absorption and scattering in the phantom skin layers

Figure 6(a) shows the absorption profiles of six different epidermis mimicking films in comparison to human epidermis measurements.[21] The absorption profiles were observed to follow a power law function, $\mu_a(\lambda) = \varphi_{\text{mel}} 1.2(\lambda/500)^{-0.7}$, with φ_{mel} ranging from 1% (very light-toned skin) to 45% (very dark-toned skin). The absorption profiles for the dermis and hypodermis mimicking layers are shown in Figs. 6(b) and 6(c) in comparison to results for human skin.[24,25] The baseline absorption due to India ink can be seen, as can the absorption peaks of the 552 nm dye in the dermis layer and the 935 nm dye in the hypodermis layer. Figures 6(d)–6(f) show scattering curves for the three skin mimicking layers in comparison to measurements on *ex vivo* human tissues.[24,25]

TABLE VI. Shear modulus, G (in kPa) of human and phantom skin, vessel wall, and blood.

Tissue layer	Phantom (kPa)	Human (kPa)	Body location (measurement technique)	Reference
Epidermis	—	~10	Abdomen (rheometry)	37
Dermis	14.43 ± 2.88 ($\gamma = 0.5$, $\dot{\gamma} = 1\ s^{-1}$)	~10	Forearm (rheometry)	38
Hypodermis	3.25 ± 0.91 ($\gamma = 0.5$, $\dot{\gamma} = 1\ s^{-1}$)	~5	Abdomen, porcine (rheometry)	38
Vessel wall	—	~75	Aorta, porcine (torsion test)	50

3.B.2. Optical properties of phantom vessels

The optical properties of the vessel wall are similar to those of dermis tissue, since the constituent materials for both tissues are similar.[52] The Sylgard 184 PDMS material in the commercial vessel tubing absorbs and scatters light minimally ($\mu_a \sim \mu_s' \sim 0\ cm^{-1}$).[53] The refractive index of Sylgard 184 PDMS is 1.40, which is comparable to that soft tissue (1.36–1.44).[23] Thus it can be assumed that the vessels are optically transparent within the phantoms.

3.B.3. Optical properties of blood mimicking fluid

The absorption spectra of venous and arterial BMF are shown in Fig. 7 in comparison to human whole blood.[54] Before the addition of the molecular dyes, absorption was substantially lower in the BMF (<1 cm^{-1}) than in human blood. After adding the dyes, the absorption peaks at 552 and 756 nm due to hemoglobin, as well as the absorption peak at 935 nm due to adipose tissue in the hypodermis, could be observed. Optical scattering in the BMF was not characterized here and will be a focus of future studies.

3.C. Phantom acoustic characterization

Speed of sound and attenuation were measured from 2 to 9 MHz. Backscatter measurements were made at 3 MHz.

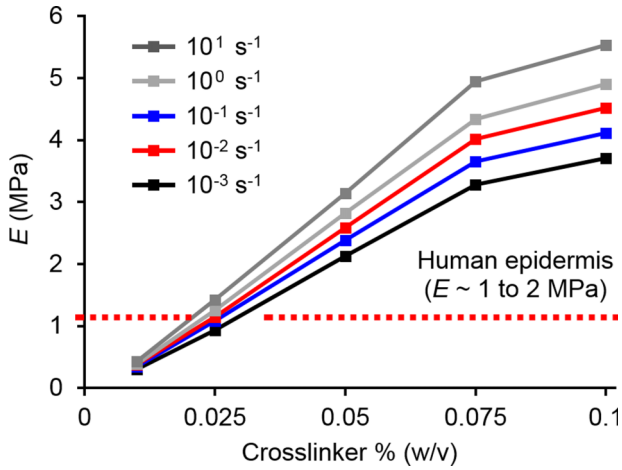

FIG. 4. Young's modulus E of epidermis mimicking gelatin sheets. The epidermis phantoms were crosslinked 0.01%–0.1% glutaraldehyde. Young's modulus was measured from tensile experiments over five strain rates. For, E was closest to that of human epidermis (~1.2 MPa, red dotted line) (Ref. 40) using 0.025% glutaraldehyde.

The specific methods used to calculate sound speeds, attenuation coefficients, and backscatter coefficients from calibrated radiofrequency pulse-echo signals have been previously described in detail.[55,56] Two single-element transducers were used for these studies. The first had a diameter of 13 mm, a center frequency of 3.8 MHz, and bandwidth of 50% (−6 dB) from 2 to 6 MHz. The second transducer had a diameter of 10 mm, a center frequency of 7.2 MHz, and bandwidth of 50% (−6 dB) from 4.5 to 9 MHz. The transducers were mounted in a water filled tank at 20.3 °C and positioned 12.75 mm (the focal distance of the transducers) above a quartz block that served as a reference reflector. For each sample, 400 pulse-echo signals were generated over a 2×2 cm area using an XYZ scanning stage. The signals were controlled by a Panametrics 5800 pulser/receiver and read by a Tektronix TDS 320 oscilloscope. The mass density of each sample was also measured. For this, a calibrated pycnometer with 0.1 mg resolution (DIN 12797, Tamson, Zoetermeer, NL) was used.

3.C.1. Acoustic properties of gelatin, IL-20, BSA, and silica microspheres

The acoustic properties of 4%, 8%, 16%, and 24% gelatin were first measured without the addition of any modifiers. 8%

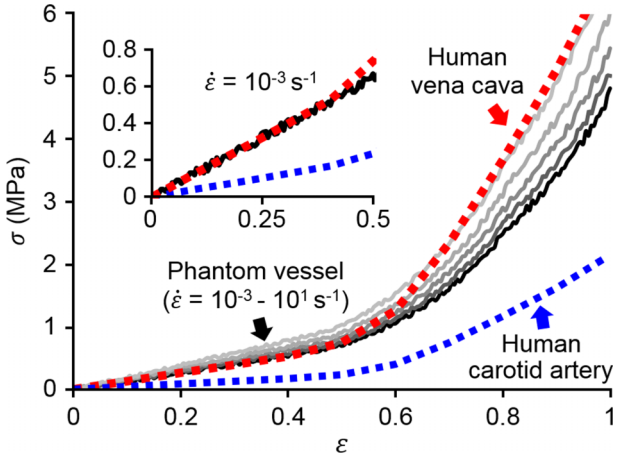

FIG. 5. Tensile stress vs strain curves for phantom vessels (solid black and grey lines) compared to *ex vivo* human adult vena cava (red dotted line) and carotid artery (blue dotted line) (Ref. 42). The lightest-colored grey line corresponds to the slowest strain rate ($\dot{\varepsilon} = 10^{-3}\ s^{-1}$) while the black line corresponds to the fastest strain rate ($\dot{\varepsilon} = 10^{1}\ s^{-1}$). The diameter of the vessels was 2 mm. Inset plot shows the linear region of stretch ($\varepsilon < 0.5$) for phantom and human vessels at comparable strain rates ($\dot{\varepsilon} = 1.0 \times 10^{-3}\ s^{-1}$ for phantom vessels, while $\dot{\varepsilon} = 1.6 \times 10^{-3}\ s^{-1}$ for human vessels). (See color online version.)

TABLE VII. Summary of optical properties of human and phantom skin, vessel wall, and blood.

Tissue layer		Absorption (μ_a), cm^{-1}			Scatter (μ_s'), cm^{-1}					Reference
		556 nm	758 nm	914 nm	556 nm	758 nm	914 nm	μ_{s_1}	n_s	
Epidermis (15% φ_{mel})	Human	53.64	23.41	14.25	60.73	42.38	34.10	68.70	1.16	21
	Phantom	49.73 ± 5.14	25.02 ± 2.93	15.06 ± 1.62	51.99 ± 12.28	29.86 ± 10.45	17.98 ± 6.78	67.01	2.11	
Dermis	Human	1.56	0.58	0.48	39.55	25.46	19.52	46.0	1.42	24
	Phantom	1.43 ± 0.19	0.50 ± 0.14	0.38 ± 0.16	38.09 ± 3.00	22.12 ± 2.33	18.01 ± 2.12	40.32	1.31	
Hypodermis	Human	1.67	0.57	0.89	17.13	13.92	12.27	18.4	0.67	25
	Phantom	1.91 ± 0.26	0.66 ± 0.18	1.05 ± 0.22	23.44 ± 2.14	13.87 ± 1.88	9.46 ± 1.05	20.01	0.87	
Vessel wall	Human	12.0	0.51	0.31	36.1	23.1	17.6	42.1	1.45	52
	Phantom	—	—	—	—	—	—	—	—	
Blood (venous)	Human	294.52	8.43	4.20	20.5	16.7	14.8	22.0	0.66	54
	Phantom	310.37 ± 4.98	9.32 ± 1.93	4.47 ± 0.76	—	—	—	—	—	
Blood (arterial)	Human	286.17	3.10	6.58	20.5	16.7	14.8	22.0	0.66	54
	Phantom	352.99 ± 3.45	2.45 ± 0.87	6.28 ± 0.51	—	—	—	—	—	

gelatin phantoms were then modified with the addition of IL-20, BSA, or silica at three different concentrations. Attenuation, backscatter, and speed of sound were observed to change linearly with concentration (Fig. 8). The attenuation coefficient α_1 of gelatin increased by 0.010 dB cm^{-1} MHz^{-1} for each percent of gelatin added. The increase in α_1 for each percent of IL-20, BSA, and silica was 0.003, 0.018, and 0.021 dB cm^{-1} MHz^{-1}, respectively [Figs. 8(a) and 8(b)]. Backscatter coefficients β_1 were low for gelatin, IL-20, and BSA (~10^{-5}–10^{-6} sr^{-1} cm^{-1} MHz^{-1}), whereas the addition of silica beads resulted in a substantially higher β_1 of ~10^{-3} sr^{-1} cm^{-1} MHz^{-1}. The backscatter power constant n_β for all four materials was ~1 [Fig. 8(c)]. The speed of sound of 8% gelatin was measured to be 1538.2 m s^{-1}. Relative to this baseline measurement, speed of sound increased by 3.57 m s^{-1} for each added percent of gelatin and 2.96 m s^{-1} for each added percent of BSA. Conversely, changes due to IL-20 and silica beads were negligible [Fig. 8(d)]. Finally, mass density increased with gelatin and BSA concentration, but did not change with IL-20 or silica bead concentration [Fig. 8(e)].

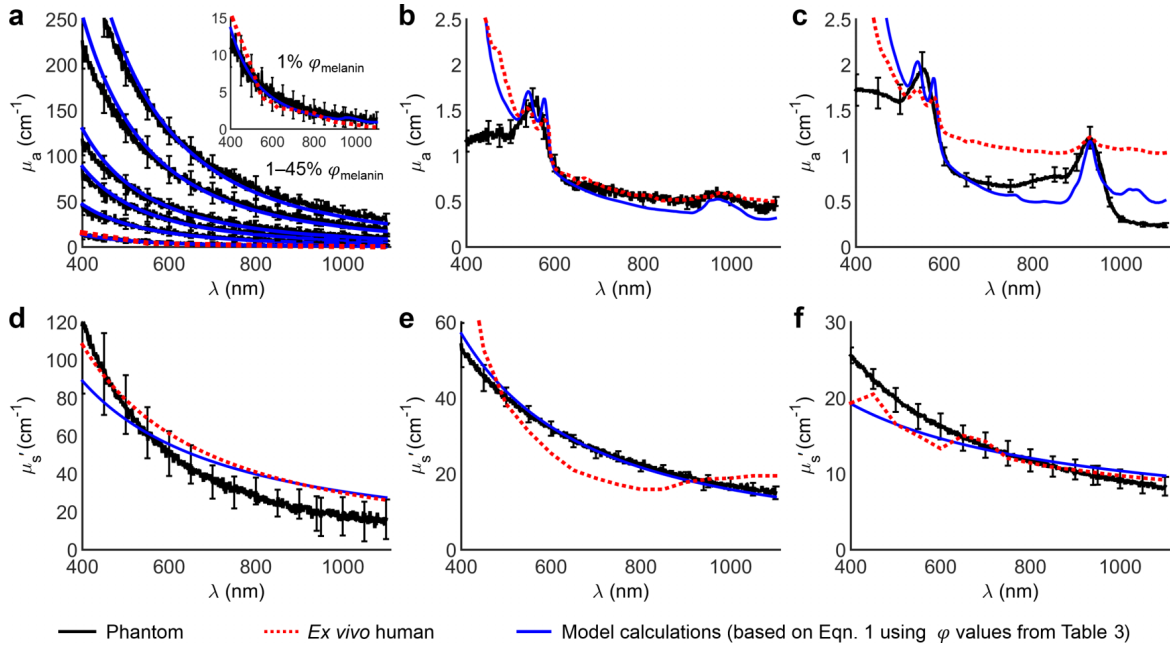

FIG. 6. Optical absorption (μ_a, top row) and reduced scattering (μ_s', bottom row) of phantom and human skin layers. (a) Absorption profiles of phantom epidermis (black lines) from 400 to 1100 nm at 1%, 5%, 10%, 15%, 30%, and 45% φ_{mel}. Absorption profiles were compared to desired model calculations (blue lines), derived using Eq. (1) with values φ taken from Table III. Also shown is the absorption curve for *ex vivo* Caucasian human epidermis (Ref. 21) (red dotted lines). Inset plot shows absorption profiles for phantom and human epidermis having 1% $\varphi_{melanin}$. [(b) and (c)] Absorption profiles of phantom dermis and hypodermis compared to model calculations and *ex vivo* human dermis (Ref. 24) and hypodermis results (Ref. 25). (d) Scattering profiles of phantom epidermis in comparison to model calculations and *ex vivo* human epidermis (Ref. 21). φ_{mel} for the phantom shown here was 15%. [(e) and (f)] Scattering profiles of phantom dermis and hypodermis compared to model calculations and *ex vivo* human measurements (Refs. 24 and 25). (See color online version.)

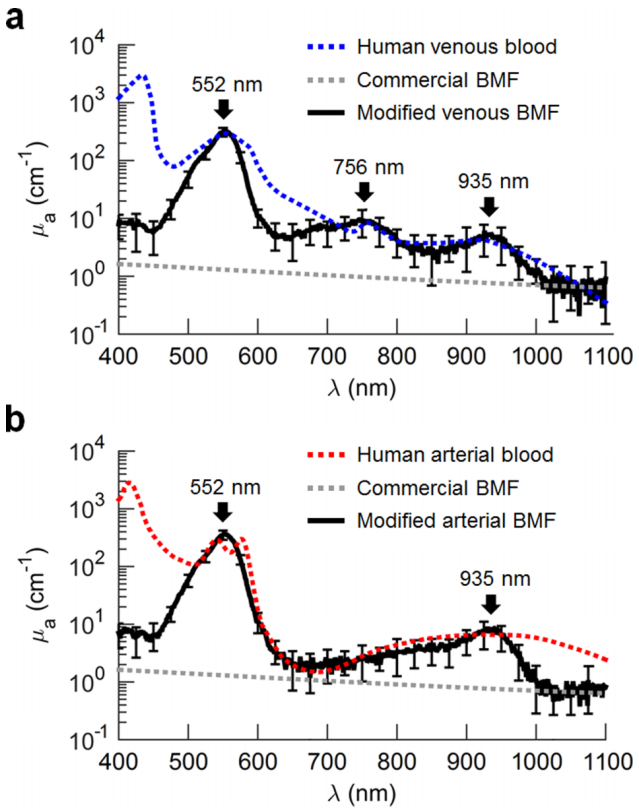

FIG. 7. Absorption of (a) venous and (b) arterial BMFs in comparison to human blood (Ref. 54). Hemoglobin absorption peaks were observed in the phantoms after the addition 552 and 756 nm dyes (black arrows). Baseline absorption provided by India ink (dotted gray lines). Four samples of venous BMF and arterial BMF were tested. The absorption of the BMF, before addition of dyes, was negligible.

3.C.2. Acoustic properties of the phantom skin layers and vessel wall

The acoustic properties of the phantoms are summarized in Table VIII and compared to the acoustic properties of human peripheral tissues. The mass densities of the phantom tissue components were comparable to the densities of the human tissues, with the largest deviation observed in the hypodermis layer. Similarly, the speed of sound in the three phantom skin layers was all within 20 m s^{-1} of the human reference data. On the other hand, the speed of sound in the PDMS material making up the vessel wall was significantly lower than the speed of sound in human vessel wall tissue, leading to a lower acoustic impedance, as discussed earlier. Attenuation in the phantom dermis, hypodermis, and vessel wall increased linearly with frequency ($n_\alpha = 1$) (Fig. 9), and the attenuation coefficients (respectively, 1.08, 0.58, and 1.14 dB cm^{-1} MHz^{-1}) closely approximated those of the human tissues. Attenuation in the epidermis layer was not measured. Backscatter coefficients of the dermis and hypodermis layers, measured at 3 MHz, ranged from 1 to 2×10^{-3} sr^{-1} cm^{-1} MHz^{-1} and were due almost entirely to the presence of silica beads. Backscatter in the epidermis was not measured, and backscatter from the PDMS material in the vessel wall was lower than the sensitivity of the instrument.

3.C.3. Acoustic properties of blood mimicking fluid

The mass density and speed of sound measurements obtained on the commercial BMF (Table VIII) were in agreement with the results reported in Ramnarine *et al.*[17,18] and are comparable to measurements on human whole blood.[33,57] The addition of molecular absorbing dyes did not cause any observable changes in the mass density or the speed of sound of the fluid. Attenuation and backscatter were below the sensitivity of the instrument.

3.D. Phantom material properties after 30 days of storage

In phantoms that were not stored under vacuum-seal, Young's modulus increased substantially after 30 days due to water loss. For phantoms stored under vacuum-seal at room temperature, no measureable changes in mechanical properties were observed after 30 days. Differences in the dermis phantoms before and after were within 1.15 kPa, which was less than the variability between samples. Similarly, differences in the hypodermis phantoms were within 0.64 kPa, which was also less than the sample variability. No measureable changes in the optical or acoustic parameters of the phantoms were observed.

3.E. Quantitative comparison of phantom and human tissue material properties

Young's modulus, optical absorption, optical scattering, and acoustic attenuation measurements obtained from the phantoms were quantitatively compared to human tissue literature data using the root mean square error (RMSE) and the normalized RMSE percent error (NRMSE%),[60] respectively, defined as

$$\mathrm{RMSE} = \sqrt{\frac{\sum_{t=1}^{n} (\hat{m} - m)^2}{n}},$$

$$\mathrm{NRMSE\%} = 100\% \times \mathrm{RMSE}/\bar{m}, \quad (1)$$

where $\hat{m}$ is the measured material property in the phantom, m is the desired material property from the human tissue data, $\bar{m}$ is the mean value for the human tissue data, and n is the number of data points. RMSE is expressed in the same units as the material property, while NRMSE% is expressed as a unitless percentage. The results are provided in Table IX.

4. DISCUSSION

While a number of previous studies have described the design of peripheral tissue phantoms, there have been relatively few reports that simultaneously consider the mechanical, optical, and acoustic properties of the skin, vessels, and blood. Invariably, multimodal phantoms containing multiple tissue types are more complicated to develop than simpler, homogenous phantoms. Challenges observed during our studies are discussed below, and future directions are outlined.

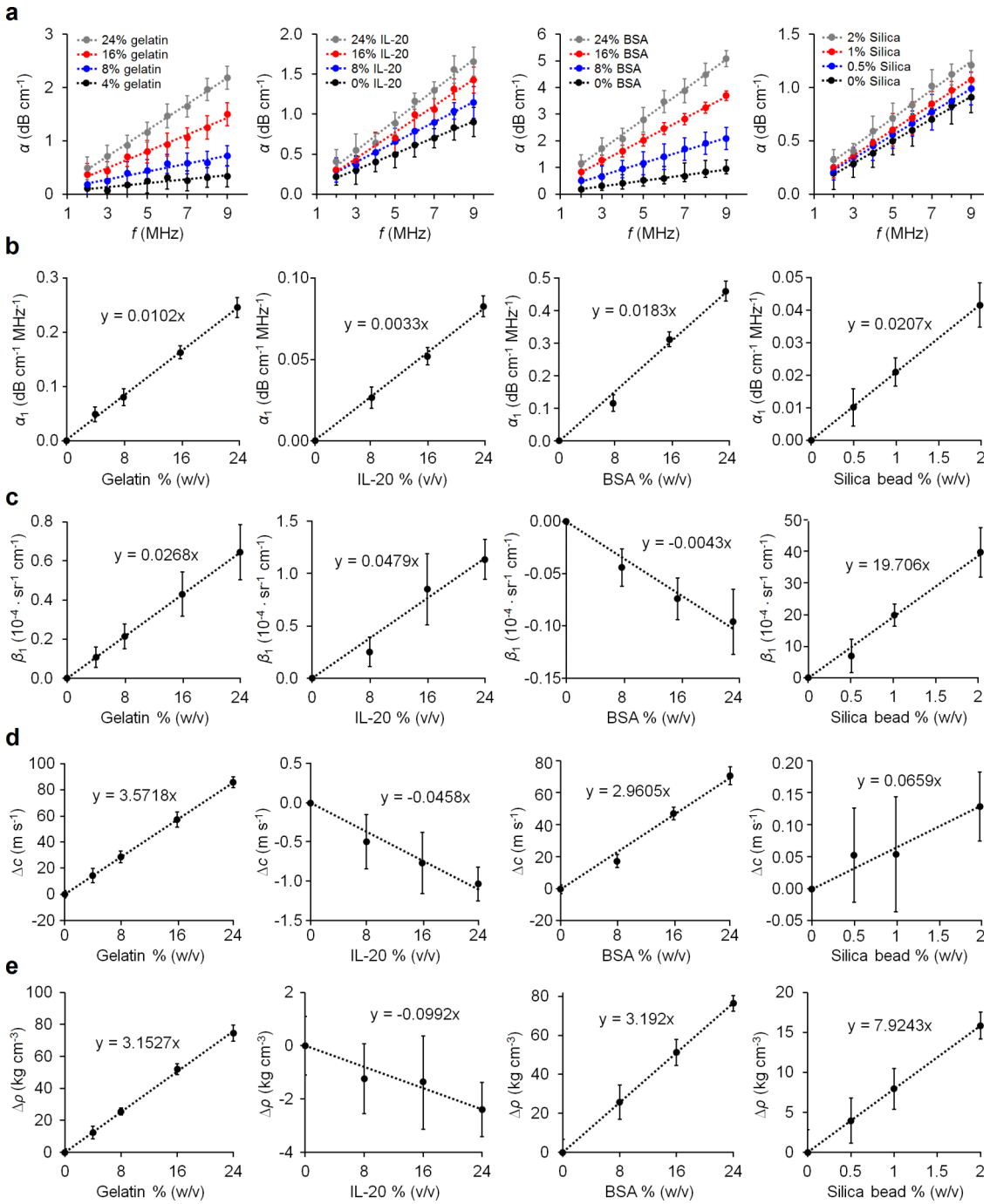

FIG. 8. Acoustic properties of gelatin, IL-20, BSA, and silica microspheres. (a) Acoustic attenuation α increased linearly with increasing concentrations of attenuating materials. Dotted lines show linear fits. Error bars show standard deviations over four replicate samples. For the plots of IL-20, BSA, and silica microspheres, black dots show attenuation of 8% gelatin phantoms without any additional modifiers, while the blue, red, and gray lines show 8% gelatin with the addition of increasing concentrations of each modifier. (b) Change in the attenuation coefficient α_1 of each material calculated from the slopes of the linear fit lines in (a). For IL-20, BSA, and silica beads, α_1 was determined after subtracting the attenuation due to 8% gelatin (black dotted lines). (c) Change in backscatter coefficients β_1 of each material from the baseline backscatter of 8% gelatin. Backascatter measurements were made at 3 MHz. (d) Change in the speed of sound c with respect to the baseline speed of sound of 8% gelatin (1538.2 m s^{-1}). (e) Change in mass density ρ. For gelatin, the change in density is shown with respect to the density of water (1000 kg m^{-3}). For IL-20, BSA, and silica beads, the changes in density are shown with respect to the baseline density of 8% gelatin (1030 kg m^{-3}). (See color online version.)

4.A. Developing custom vessel tubing

In the commercial PDMS vessel tubing, speed of sound and thus acoustic impedance were both reduced compared to human vessel tissue, leading to uncharacteristic acoustic reflections at the phantom vessel wall. An alternative to using commercial tubing is to fabricate customized vessels, which would greatly increase the material choices and allow for the addition of modifiers. Some fabrication approaches have been reported. For example, the mechanical properties of

TABLE VIII. Summary of acoustic properties of human and phantom skin, vessel wall, and blood.

Tissue layer		ρ (kg m^{-3})	c (m s^{-1})	Z ($10^6 \cdot$kg m^{-2} s^{-1})	α_1 (dB cm^{-1} MHz^{-1})	n_α	β_1 (10^{-4} sr^{-1} cm^{-1} MHz^{-1})	n_β	References
Epidermis	Human	1233	1645	1.99	0.44	1.6	~50	3.8	34
	Phantom	1250.8 ± 14.1	1625.3 ± 9.71	2.03 ± 0.035	—	—	—	—	
Dermis	Human	1151	1595	1.8	0.26	1.7	~20	2.8	34
	Phantom	1064.2 ± 4.2	1593.1 ± 6.32	1.70 ± 0.013	1.08 ± 0.23	1.0	19.7 ± 4.2	1.0	
Hypodermis	Human	928	1450	1.38	0.60	1.0	~5	1.0	33
	Phantom	1035.1 ± 6.3	1443.0 ± 5.55	1.49 ± 0.015	0.58 ± 0.19	1.0	8.1 ± 2.5	1.0	
Vessel wall	Human	1065	1600	1.70	1.50	0.9	~20	1.6	58 and 59
	Phantom	1030.1 ± 3.5	1089.2 ± 2.24	1.12 ± 0.006	1.14 ± 0.16	1.0	—	—	
Blood	Human	1050	1584	1.66	0.15	1.2	~0.1	3.5	17 and 57
	Phantom	1037.4 ± 4.8	1578.4 ± 5.15	1.64 ± 0.010	—	—	—	—	

PDMS may be controlled by varying the ratio of elastomer and curing agent, or by curing at different temperatures.[12] Materials other than PDMS, including polyvinyl alcohol and hydrogels, may also be used.[13,15,16] Of particular interest are vessel substitutes fabricated from gelatin or agar, since these materials can accommodate the modifiers discussed in this paper as well as many others. Our group is looking into developing gelatin-based vessels using 3D-printed molds that define the vessel diameter and wall thickness. Such vessels, if fabricated in a convenient manner, would greatly increase the customizability of the phantoms as a whole.

4.B. Rationale for characterizing each phantom tissue component independently rather than as a composite

To allow direct comparisons to literature data on human tissues, the five phantom tissue components were assessed independently. Because the individual components were homogenous, each could be tested using conventional experimental approaches. In contrast, evaluating the behavior of the multilayered composite phantom would likely have required more complex material models and techniques.[61–63] In future studies, such approaches may be implemented to allow the composite material properties of the phantoms to be characterized.

4.C. Reliability of reference data obtained from *ex vivo* tissues

A combination of *in vivo* and *ex vivo* human tissue reference values were used in this study. For some properties (e.g., Young's modulus, optical absorption, and optical scattering), *in vivo* measurements obtained with conventional testing methods were not easily found. Here, *ex vivo* data were used because the same testing methods could be implemented on the phantoms, thereby allowing direct comparisons between the phantom and human tissue results. For example, the uniaxial stress vs strain results on the phantom skin layers and vessels could be directly compared only to *ex vivo* data, since conventional stress vs strain tests are difficult or impossible to implement *in vivo*. The *ex vivo* measurements used here for reference were obtained under well-controlled experimental conditions, and detailed descriptions were provided of the steps taken to minimize changes in the tissue samples after excision. In most of the referenced studies, samples were maintained in saline at either physiological or room temperature for no more than a few hours before testing, and

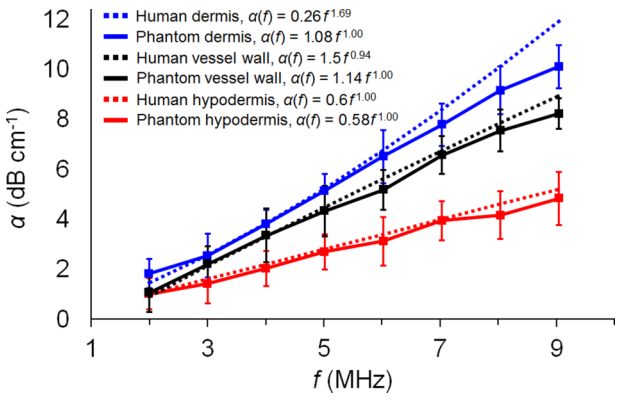

FIG. 9. Acoustic attenuation α of phantom dermis, hypodermis, and vessel wall (solid lines) in the frequency range of 2–9 MHz compared to human data from the literature (dotted lines) (Refs. 33, 34, and 58). The power law parameters α_1 and n_α are also shown for each tissue.

TABLE IX. RMSEs and normalized RMSE % errors (parentheses) for Young's modulus, optical absorption, optical scattering, and acoustic attenuation measurements in comparison to human tissue data.

	E (kPa)	μ_a (cm^{-1})	μ_s' (cm^{-1})	α (dB cm^{-1})
Epidermis	0.11×10^3 (7.75%)	3.73 (4.23%)	6.60 (6.16%)	N/A
Dermis	1.02 (2.21%)	0.13 (8.11%)	2.68 (6.80%)	1.94 (5.79%)
Hypodermis	0.07 (3.95%)	0.17 (9.82%)	1.73 (9.73%)	1.05 (9.04%)
Vessel wall	0.04×10^3 (1.06%)	N/A	N/A	1.54 (6.14%)
Blood	N/A	17.75 (7.88%)	N/A	N/A

measurements were found to be in agreement with prior *in vivo* results.

4.D. Evaluating phantom stability and longevity over several months

Germall-Plus was used as the antimicrobial in our phantoms, all of which were packaged and stored in vacuum-sealed bags. No measureable changes in mechanical properties were observed after 30 days at room temperature. The stability of the phantoms after 30 days was not assessed. Madsen *et al.* have previously shown that, in properly stored gelatin and agar phantoms incorporating Germall-Plus, mechanical properties remain stable over a 7–10 month period.[9] In follow-up studies, the phantoms' material properties will be evaluated over similar time durations.

5. CONCLUSION

In this paper, we have described the design, fabrication, and characterization of tissue mimicking phantoms that reproduce the mechanical, optical, and acoustic properties of five peripheral tissues, namely, the epidermis, dermis, hypodermis, blood vessels, and blood. The mechanical properties included the tissue thickness or diameter, Young's modulus, and dynamic shear modulus at strains below 0.5. The optical properties included the optical absorption and scattering at wavelengths of 400–1100 nm. Finally the acoustic properties included the acoustic attenuation and backscatter at frequencies of 2–9 MHz. The phantoms are uniquely suited to serve as test models for multimodal skin and vascular imaging techniques and image-guided interventions.

NOMENCLATURE

δ	thickness (mm)
d	diameter (mm)
E	Young's modulus (kPa)
G	shear modulus (kPa)
σ	uniaxial stress (kPa)
ε	uniaxial strain (unitless)
$\dot{\varepsilon}$	uniaxial strain rate (s^{-1})
τ	shear stress (kPa)
γ	shear strain (unitless)
$\dot{\gamma}$	shear strain rate (s^{-1})
η	viscosity (kg m^{-1} s^{-1})
μ_a	optical absorption coefficient (cm^{-1})
μ_s	optical scattering coefficient (cm^{-1})
μ_s'	optical reduced scattering coefficient (cm^{-1})
λ	wavelength (nm)
φ	percent volume fraction (%)
ρ	mass density (kg m^{-3})
c	velocity of sound (m s^{-1})
Z	acoustic impedance (10^6 kg m^{-2} s^{-1})
α	acoustic attenuation (dB cm^{-1})
β	acoustic backscatter (sr^{-1} cm^{-1})
f	frequency (MHz)

CONFLICT OF INTEREST DISCLOSURE

The authors have no relevant conflicts of interest to disclose.

[a]Author to whom correspondence should be addressed. Electronic mail: alvin.chen@rutgers.edu

[1]M. Xu and L. V. Wang, "Photoacoustic imaging in biomedicine," Rev. Sci. Instrum. **77**(4), 041101 (2006).
[2]A. Sarvazyan, T. J. Hall, M. W. Urban, M. Fatemi, S. R. Aglyamov, and B. S. Garra, "An overview of elastography-an emerging branch of medical imaging," Curr. Med. Imaging Rev. **7**(4), 255–282 (2011).
[3]K. Cleary and T. Peters, "Image-guided interventions: Technology review and clinical applications," Annu. Rev. Biomed. Eng. **12**, 119–142 (2010).
[4]B. W. Pogue and M. S. Patterson, "Review of tissue simulating phantoms for optical imaging," J. Biomed. Opt. **11**(4), 041102 (2006).
[5]M. O. Culjat, D. Goldenberg, P. Tewari, and R. S. Singh, "A review of tissue substitutes for ultrasound imaging," Ultrasound Med. Biol. **36**(6), 861–873 (2010).
[6]T. J. Hall, M. Bilgen, M. F. Insana, and T. A. Krouskop, "Phantom materials for elastography," IEEE Trans. Ultrason., Ferroelectr., Freq. Control **44**(6), 1355–1365 (1997).
[7]G. Lamouche, B. F. Kennedy, K. M. Kennedy, C.-E. Bisaillon, A. Curatolo, G. Campbell, V. Pazos, and D. D. Sampson, "Review of tissue simulating phantoms with controllable optical, mechanical and structural properties for use in optical coherence tomography," Biomed. Opt. Express **3**(6), 1381–1398 (2012).
[8]E. L. Madsen, J. A. Zagzebski, R. A. Banjavie, and R. E. Jutila, "Tissue mimicking materials for ultrasound phantoms," Med. Phys. **5**(5), 391–394 (1978).
[9]E. L. Madsen, M. A. Hobson, H. Shi, T. Varghese, and G. R. Frank, "Tissue-mimicking agar/gelatin materials for use in heterogeneous elastography phantoms," Phys. Med. Biol. **50**(23), 5597–5618 (2005).
[10]J. R. Cook, R. R. Bouchard, and S. Y. Emelianov, "Tissue-mimicking phantoms for photoacoustic and ultrasonic imaging," Biomed. Opt. Express **2**(11), 3193–3206 (2011).
[11]N. Hungr, J. A. Long, V. Beix, and J. Troccaz, "A realistic deformable prostate phantom for multimodal imaging and needle-insertion procedures," Med. Phys. **39**(4), 2031–2041 (2012).
[12]T. L. Poepping, H. N. Nikolov, M. L. Thorne, and D. W. Holdsworth, "A thin-walled carotid vessel phantom for Doppler ultrasound flow studies," Ultrasound Med. Biol. **30**(8), 1067–1078 (2004).
[13]K. J. Surry, H. J. Austin, A. Fenster, and T. M. Peters, "Poly (vinyl alcohol) cryogel phantoms for use in ultrasound and MR imaging," Phys. Med. Biol. **49**(24), 5529–5546 (2004).
[14]D. M. King, C. M. Moran, J. D. McNamara, A. J. Fagan, and J. E. Browne, "Development of a vessel-mimicking material for use in anatomically realistic Doppler flow phantoms," Ultrasound Med. Biol. **37**(5), 813–826 (2011).
[15]C. L. de Korte, E. I. Céspedes, A. F. van der Steen, B. Norder, and K. te Nijenhuis, "Elastic and acoustic properties of vessel mimicking material for elasticity imaging," Ultrason. Imaging **19**(2), 112–126 (1997).
[16]L. K. Ryan and F. S. Foster, "Tissue equivalent vessel phantoms for intravascular ultrasound," Ultrasound Med. Biol. **23**(2), 261–273 (1997).
[17]K. V. Ramnarine, D. K. Nassiri, P. R. Hoskins, and J. Lubbers, "Validation of a new blood-mimicking fluid for use in Doppler flow test objects," Ultrasound Med. Biol. **24**(3), 451–459 (1998).
[18]K. V. Ramnarine, P. R. Hoskins, H. F. Routh, and F. Davidson, "Doppler backscatter properties of a blood-mimicking fluid for Doppler performance assessment," Ultrasound Med. Biol. **25**(1), 105–110 (1999).
[19]S. L. Jacques, "Optical properties of biological tissues: A review," Phys. Med. Biol. **58**(11), R37–R61 (2013).
[20]W. F. Cheong, S. A. Prahl, and A. J. Welch, "A review of the optical properties of biological tissues," IEEE J. Quantum Electron. **26**(12), 2166–2185 (1990).
[21]E. Salomatina, B. Jiang, J. Novak, and A. N. Yaroslavsky, "Optical properties of normal and cancerous human skin in the visible and near-infrared spectral range," J. Biomed. Opt. **11**(6), 064026 (2006).
[22]A. N. Bashkatov, E. A. Genina, V. F. Kochubey, M. M. Stolnitz, T. A. Bashkatova, O. V. Novikova, A. Y. Peshkova, and V. V. Tuchin, "Optical properties of melanin in the skin and skin-like phantoms," Proc. SPIE **4162**, 219–226 (2000).

[23]H. Ding, J. Q. Lu, W. A. Wooden, P. J. Kragel, and X. H. Hu, "Refractive indices of human skin tissues at eight wavelengths and estimated dispersion relations between 300 and 1600 nm," Phys. Med. Biol. **51**(6), 1479–1489 (2006).
[24]A. N. Bashkatov, E. A. Genina, V. I. Kochubey, and V. V. Tuchin, "Optical properties of human skin, subcutaneous and mucous tissues in the wavelength range from 400 to 2000 nm," J. Phys. D: Appl. Phys. **38**(15), 2543–2555 (2005).
[25]A. N. Bashkatov, "Optical properties of the subcutaneous adipose tissue in the spectral range 400–2500 nm," Opt. Spectrosc. **99**(5), 836–842 (2005).
[26]P. Di Ninni, F. Martelli, and G. Zaccanti, "The use of India ink in tissue-simulating phantoms," Opt. Express **18**(26), 854–865 (2010).
[27]P. Di Ninni, F. Martelli, and G. Zaccanti, "Intralipid: Towards a diffusive reference standard for optical tissue phantoms," Phys. Med. Biol. **56**(2), N21–N28 (2011).
[28]L. Spinelli, M. Botwicz, N. Zolek, M. Kacprzak, D. Milej, P. Sawosz, A. Liebert, U. Weigel, T. Durduran, F. Foschum, A. Kienle, F. Baribeau, S. Leclair, J. P. Bouchard, I. Noiseux, P. Gallant, O. Mermut, A. Farina, A. Pifferi, A. Torricelli, R. Cubeddu, H. C. Ho, M. Mazurenka, H. Wabnitz, K. Klauenberg, O. Bodnar, C. Elster, M. Bénazech-Lavoué, Y. Bérubé-Lauzière, F. Lesage, D. Khoptyar, A. A. Subash, S. Andersson-Engels, P. Di Ninni, F. Martelli, and G. Zaccanti, "Determination of reference values for optical properties of liquid phantoms based on intralipid and India ink," Biomed. Opt. Express **5**(7), 2037–2053 (2014).
[29]K. K. Shung, *Ultrasonic Scattering in Biological Tissues* (CRC Press, Inc., Florida, 1993).
[30]K. Zell, J. I. Sperl, M. W. Vogel, R. Niessner, and C. Haisch, "Acoustical properties of selected tissue phantom materials for ultrasound imaging," Phys. Med. Biol. **52**(20), N475–N488 (2007).
[31]C. Lafon, V. Zderic, M. L. Noble, J. C. Yuen, P. J. Kaczkowski, O. A. Sapozhnikov, F. Chavrier, L. A. Crum, and S. Vaezy, "Gel phantom for use in high-intensity focused ultrasound dosimetry," Ultrasound Med. Biol. **31**(10), 1383–2053 (2005).
[32]O. A. Ejofodomi, V. Zderic, and J. M. Zara, "Tissue-mimicking bladder wall phantoms for evaluating acoustic radiation force-optical coherence elastography systems," Med. Phys. **37**(4), 1440–1448 (2010).
[33]H. Azhari, *Basics of Biomedical Ultrasound for Engineers* (John Wiley & Sons, Inc., New York, 2010), pp. 313–314.
[34]C. M. Moran, N. L. Bush, and J. C. Bamber, "Ultrasonic propagation properties of excised human skin," Ultrasound Med. Biol. **21**(9), 1177–1190 (1995).
[35]O. A. Shergold, N. A. Fleck, and D. Radford, "The uniaxial stress versus strain response of pig skin and silicone rubber at low and high strain rates," Int. J. Impact Eng. **32**(9), 1384–1402 (2006).
[36]K. Comley and N. Fleck, "The compressive response of porcine adipose tissue from low to high strain rate," Int. J. Impact Eng. **46**, 1–10 (2012).
[37]M. Geerligs, C. Oomens, P. Ackermans, F. Baaijens, and G. Peters, "Linear shear response of the upper skin layers," Biorheology **48**(3), 229–245 (2011).
[38]M. Geerligs, G. W. Peters, P. A. Ackermans, C. W. Oomens, and F. P. Baaijens, "Linear viscoelastic behavior of subcutaneous adipose tissue," Biorheology **45**(6), 677–688 (2008).
[39]J. Sandby-Møller, T. Poulsen, and H. C. Wulf, "Epidermal thickness at different body sites: Relationship to age, gender, pigmentation, blood content, skin type and smoking habits," Acta Derm.-Venereol. **83**(6), 410–413 (2003).
[40]M. Geerligs, L. van Breemen, G. Peters, P. Ackermans, F. Baaijens, and C. Oomens, "*In vitro* indentation to determine the mechanical properties of epidermis," J. Biomech. **44**(6), 1176–1181 (2011).
[41]F. M. Hendriks, D. Brokken, C. W. Oomens, D. L. Bader, and F. P. Baaijens, "The relative contributions of different skin layers to the mechanical behavior of human skin *in vivo* using suction experiments," Med. Eng. Phys. **28**(3), 259–266 (2006).
[42]F. H. Silver, P. B. Snowhill, and D. J. Foran, "Mechanical behavior of vessel wall: A comparative study of aorta, vena cava, and carotid artery," Ann. Biomed. Eng. **31**(7), 793–803 (2003).
[43]S. Diridollou, F. Patat, F. Gens, L. Vaillant, D. Black, J. M. Lagarde, Y. Gall, and M. Berson, "*In vivo* model of the mechanical properties of the human skin under suction," Skin Res. Technol. **6**(4), 214–221 (2000).
[44]J. L. Gennisson, T. Baldeweck, M. Tanter, S. Catheline, M. Fink, L. Sandrin, C. Cornillon, and B. Querleux, "Assessment of elastic parameters of human skin using dynamic elastography," IEEE Trans. Ultrason., Ferroelectr., Freq. Control **51**(8), 980–989 (2004).
[45]S. Diridollou, M. Berson, V. Vabre, D. Black, B. Karlsson, F. Auriol, J. M. Gregoire, C. Yvon, L. Vaillant, Y. Gall, and F. Patat, "An *in vivo* method for measuring the mechanical properties of the skin using ultrasound," Ultrasound Med. Biol. **24**(2), 215–224 (1998).
[46]F. M. Hendriks, D. Brokken, J. T. van Eemeren, C. W. Oomens, F. P. Baaijens, and J. B. Horsten, "A numerical-experimental method to characterize the non-linear mechanical behaviour of human skin," Skin Res. Technol. **9**(3), 274–283 (2003).
[47]C. Y. Tan, B. Statham, R. Marks, and P. A. Payne, "Skin thickness measurement by pulsed ultrasound: Its reproducibility, validation and variability," Br. J. Dermatol. **106**(6), 657–667 (1982).
[48]J. G. Jacot, I. Abdullah, M. Belkin, M. Gerhard-Herman, P. Gaccione, J. F. Polak, M. C. Donaldson, A. D. Whittemore, and M. S. Conte, "Early adaptation of human lower extremity vein grafts: Wall stiffness changes accompany geometric remodeling," J. Vasc. Surg. **39**(3), 547–555 (2004).
[49]C. Pailler-Mattei, S. Bec, and H. Zahouani, "*In vivo* measurements of the elastic mechanical properties of human skin by indentation tests," Med. Eng. Phys. **30**(5), 599–606 (2008).
[50]J. Vossoughi and A. Tozeren, "Determination of an effective shear modulus of aorta," Russ. J. Biomech. **1**(2), 20–36 (1998).
[51]S. A. Prahl, M. J. van Gemert, and A. J. Welch, "Determining the optical properties of turbid media by using the adding-doubling method," Appl. Opt. **32**(4), 559–568 (1993).
[52]M. J. van Gemert, R. Verdaasdonk, E. G. Stassen, G. A. Schets, G. H. Gijsbers, and J. J. Bonnier, "Optical properties of human blood vessel wall and plaque," Lasers Surg. Med. **5**(3), 235–237 (1985).
[53]S. Deguchi, J. Hotta, S. Yokoyama, and T. Matsui, "Viscoelastic and optical properties of four different PDMS polymers," J. Micromech. Microeng. **25**(9), 097002 (2015).
[54]A. Roggan, M. Friebel, K. Dörschel, A. Hahn, and G. Müller, "Optical properties of circulating human blood in the wavelength range 400–2500 nm," J. Biomed. Opt. **4**(1), 36–46 (1999).
[55]J. F. Chen, J. A. Zagzebski, and E. L. Madsen, "Tests of backscatter coefficient measurements using broadband pulses," IEEE Trans. Ultrason., Ferroelectr., Freq. Control **40**(5), 603–607 (1993).
[56]E. L. Madsen, F. Dong, G. R. Frank, B. S. Garra, K. A. Wear, T. Wilson, J. A. Zagzebski, H. L. Miller, K. K. Shung, S. H. Wang, E. J. Feleppa, T. Liu, W. D. O'Brien, K. A. Topp, N. T. Sanghvi, A. V. Zaitsev, T. J. Hall, J. B. Fowlkes, O. D. Kripfgans, and J. G. Miller, "Interlaboratory comparison of ultrasonic backscatter, attenuation, and speed measurements," J. Ultrasound Med. **18**(9), 615–631 (1999).
[57]Y. W. Yuan, "Ultrasonic backscatter from flowing whole blood: Dependence on shear rate and hematocrit," J. Acoust. Soc. Am. **84**(1), 52–58 (1988).
[58]K. H. Fraser, T. L. Poepping, A. McNeilly, I. L. Megson, and P. R. Hoskins, "Acoustic speed and attenuation coefficient in sheep aorta measured at 5-9 MHz," Ultrasound Med. Biol. **32**(6), 971–980 (2006).
[59]G. R. Lockwood, L. K. Ryan, J. W. Hunt, and F. S. Foster, "Measurement of the ultrasonic properties of vascular tissues and blood from 35-65 MHz," Ultrasound Med. Biol. **17**(7), 653–666 (1991).
[60]J. Law and R. Rennie, *A Dictionary of Physics*, 7th ed. (Oxford University Press, Oxford, 2009), pp. 192–193.
[61]M. Freutel, H. Schmidt, L. Dürselen, A. Ignatius, and F. Galbusera, "Finite element modeling of soft tissues: Material models, tissue interaction and challenges," Clin. Biomech. **29**(4), 363–372 (2014).
[62]B. E. Treeby, J. Jaros, A. P. Rendell, and B. T. Cox, "Modeling nonlinear ultrasound propagation in heterogeneous media with power law absorption using a k-space pseudospectral method," J. Acoust. Soc. Am. **131**, 4324–4336 (2012).
[63]L. H. Wang, S. L. Jacques, and L. Q. Zheng, "MCML—Monte Carlo modeling of light transport in multi-layered tissues," Comput. Methods Programs Biomed. **47**(2), 131–146 (1995).